

Properties of the Magellanic Corona

SCOTT LUCCHINI ^{1,2} ELENA D'ONGHIA ^{2,3} AND ANDREW J. FOX ^{4,5}

¹*Center for Astrophysics — Harvard & Smithsonian, 60 Garden St, Cambridge, MA, USA*

²*Department of Physics, University of Wisconsin - Madison, Madison, WI, USA*

³*Department of Astronomy, University of Wisconsin - Madison, Madison, WI, USA*

⁴*AURA for ESA, Space Telescope Science Institute, 3700 San Martin Drive, Baltimore, MD, USA*

⁵*Department of Physics & Astronomy, Johns Hopkins University, 3400 N. Charles Street, Baltimore, MD 21218, USA*

ABSTRACT

We characterize the Magellanic Corona, the warm gaseous halo around the Large Magellanic Cloud (LMC). The Corona is a key ingredient in the formation of the Magellanic Stream (Lucchini et al. 2020, 2021) and has recently been observed in high-ion absorption around the LMC. In this work we present a suite of high-resolution hydrodynamical simulations to constrain its total mass and temperature prior to the infall of the Magellanic Clouds to our Galaxy. We find that the LMC is able to host a stable Corona before and during its approach to the MW through to the present day. With a Magellanic Corona of $> 2 \times 10^9 M_{\odot}$ at 3×10^5 K, our simulations can reproduce the observed total mass of the neutral and ionized components of the Trailing Stream, size of the LMC disk, ionization fractions along the Stream, morphology of the neutral gas, and on-sky extent of the ionized gas. The Corona plays an integral role in the survival, morphology, and composition of the Magellanic Clouds and the Trailing Stream.

Keywords: Galactic and extragalactic astronomy (563) – Galaxy dynamics (591) – Galaxy physics (612) – Magellanic Clouds (990) – Magellanic Stream (991) – Milky Way Galaxy (1054)

1. INTRODUCTION

The Magellanic Stream is the largest coherent extragalactic gaseous structure in our sky (Mathewson et al. 1974). It has the potential to dramatically impact the future of the Milky Way (MW) by depositing billions of solar masses of gas into our circumgalactic medium (CGM) and possibly onto our disk (Fox et al. 2014; D’Onghia & Fox 2016). The Magellanic Stream also provides direct evidence of galaxy interactions and evolution through mergers. By studying this serendipitous nearby system, we will learn about the future of our own Galaxy, the history of the Local Group, and the gas and metal transport processes that can sustain the growth of galaxies like the MW.

The Magellanic Stream is an extended network of interwoven clumpy filaments of gas that originate from within the Large and Small Magellanic Clouds (LMC, SMC), two satellite galaxies of the MW. Combined with

the Leading Arm, high velocity clumps of gas ahead of the Magellanic Clouds in their orbits, the Magellanic System covers over 200° on the sky. From 21-cm H I observations, we have a detailed view of its small-scale, turbulent morphology as well as its velocity structure (e.g. Cohen 1982; Morras 1983; Putman et al. 2003; Brüns et al. 2005; Nidever et al. 2008, 2010; Westmeier 2018). Moreover, absorption-line spectroscopy studies have characterized the chemical composition and ionization state of the Stream along dozens of sightlines (Lu et al. 1994; Gibson et al. 2000; Sembach et al. 2003; Fox et al. 2010, 2013, 2014; Richter et al. 2013). Fox et al. (2014) has shown that the Stream is mostly ionized. They find an average ionization fraction of $\approx 73\%$ with a total ionized gas mass of $\sim 1.5 \times 10^9 M_{\odot}$ (compared with $4.9 \times 10^8 M_{\odot}$ of neutral gas; Brüns et al. 2005).

Models of the formation of the Stream originally explained the stripped material as gas that was tidally pulled from the LMC through repeated interactions with the MW (Fujimoto & Sofue 1976; Davies & Wright 1977; Lin & Lynden-Bell 1977, 1982; Gardiner & Noguchi

1996; Connors et al. 2006; Diaz & Bekki 2011). This would result not only in stripped gas, but also in a tidally truncated dark matter halo. Thus, masses determined by rotation curve fitting ($1.7 \pm 0.7 \times 10^{10} M_{\odot}$ within 8.7 kpc, van der Marel & Kallivayalil 2014) would be sufficient for modeling the evolution of the Clouds and the formation of the Stream. However, updated proper-motion measurements of the LMC and SMC have shown that the Clouds are most likely on their first infall towards the Milky Way (Kallivayalil et al. 2006; Besla et al. 2007; Kallivayalil et al. 2013). A recent study has found a second passage orbit consistent with the observations, however further studies of the hydrodynamics are required to see if the Stream can be reproduced (Vasiliev 2024). A first-infall scenario would require a higher LMC mass as it would not yet be tidally truncated.

Many different indirect methods of estimating the LMC’s total pre-infall mass have converged on a value of $1 - 2 \times 10^{11} M_{\odot}$: $1.98 \times 10^{11} M_{\odot}$ from abundance matching (Read & Erkal 2019), $>10^{11} M_{\odot}$ from the MW’s reflex motion (Petersen & Peñarrubia 2021), $>1.24 \times 10^{11} M_{\odot}$ from the LMC’s satellite population (Erkal & Belokurov 2020), $2.5^{+0.09}_{-0.08} \times 10^{11} M_{\odot}$ from the Hubble flow timing argument (Peñarrubia et al. 2016), and $1.3 \pm 0.3 \times 10^{11}$ and $1.38^{+0.27}_{-0.24} \times 10^{11} M_{\odot}$ from the Sagittarius (Vasiliev et al. 2021) and Orphan-Chenab Streams (Erkal et al. 2019), respectively. See Figure 1 for a summary of these measurements. We include the error-weighted mean of the values calculated in Watkins et al. (2024), Vasiliev et al. (2021), Erkal et al. (2019), Read & Erkal (2019), and Peñarrubia et al. (2016): $1.55 \pm 0.26 \times 10^{11} M_{\odot}$ ($\sim 10 - 20\%$ of the MW’s total mass)¹.

While modern tidal models of the formation of the Stream have used large masses for the LMC, they are unable to explain the immense mass of ionized gas ($> 10^9 M_{\odot}$ Besla et al. 2010, 2012; Pardy et al. 2018). On the other hand, ram pressure models (Meurer et al. 1985; Moore & Davis 1994; Sofue 1994) are able to explain the ionized material via dissolution of the neutral gas through instabilities, but they require low masses for the LMC ($< 2 \times 10^{10} M_{\odot}$; Hammer et al. 2015; Wang et al. 2019).

¹ We note that some of these methods do depend on the assumed MW total mass, which is uncertain at the $\sim 30\%$ level (Bland-Hawthorn & Gerhard 2016). However, each of the references listed above have simultaneously constrained the MW and LMC mass to reach the values quoted. Moreover, even reducing the LMC mass estimates by 30% leaves our average value above $10^{11} M_{\odot}$.

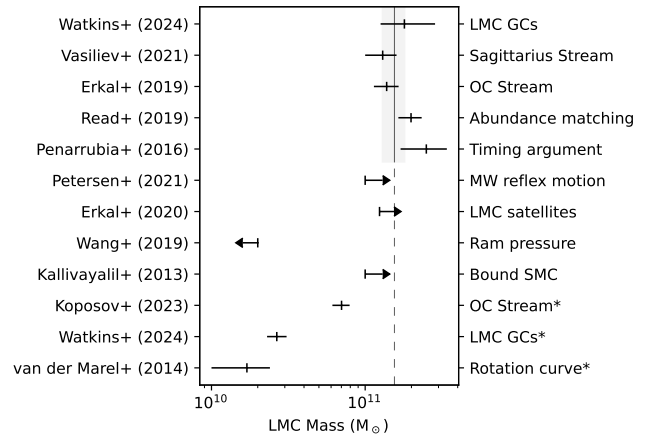


Figure 1. Observational LMC total mass estimates. Literature estimates for the total mass of the Large Magellanic Cloud. van der Marel & Kallivayalil (2014) and Koposov et al. (2023) (denoted with asterisks) provide constraints on the mass within 8.7 and 32.4 kpc, respectively, while Watkins et al. (2024) provides a direct constraint within 13.2 kpc (second from the bottom) in addition to a fit using an NFW profile (top). All other estimates plotted are for the total virial LMC mass. Kallivayalil et al. (2013), Erkal & Belokurov (2020), and Petersen & Peñarrubia (2021) provide lower limits, and Wang et al. (2019) provide an upper limit. The remaining references (Peñarrubia et al. 2016; Read & Erkal 2019; Erkal et al. 2019; Vasiliev et al. 2021; Watkins et al. 2024) give estimates of the total LMC mass with uncertainties. The error weighted average of these five values is $1.55 \pm 0.26 \times 10^{11} M_{\odot}$ shown as the vertical line (extended to the bottom of the plot as a dashed line for comparison). The one-sigma errors are shown as a shaded region. The method for determining the LMC mass estimate from each paper is listed on the right edge of the plot.

To resolve both of these discrepancies simultaneously, we introduced the Magellanic Corona model (Lucchini et al. 2020, 2021, hereafter L20, L21). Based on theoretical calculations and cosmological simulations, galaxies with masses $\sim 10^{11} M_{\odot}$ should host gaseous halos at or near their virial temperature of $\sim 3 \times 10^5 K^2$ (Jahn et al. 2021). Upon inclusion of a warm CGM around the LMC, dubbed the Magellanic Corona, we are able to explain the ionized material in the Stream while accounting for a massive LMC. In L21, we showed that this Magellanic Corona also exerts hydrodynamical drag on the SMC as it orbits around the LMC. With a new orbital history consistent with the present-day positions and velocities of the Clouds, the Trailing Stream ends up several times closer to us than previous models predicted.

² While this value is near the peak of the interstellar cooling curve, the Corona can remain stable if heated (e.g. through supernova feedback). See Figure 4.

Table 1. Initial Galaxy Properties in the simulations

	LMC ($t = 0$ Gyr)	SMC	MW
DM Mass (M_{\odot})	1.75×10^{11}	5×10^9	1.1×10^{12}
Stellar Disk Mass (M_{\odot})	2.5×10^9	2.5×10^8	–
Stellar Scale Length (kpc)	4.5	1.7	–
Gaseous Disk Mass (M_{\odot})	0	1.5×10^9	–
Gaseous Scale Length (kpc)	–	6.9	–
CGM Mass ^a (M_{\odot})	$10^9 - 10^{10}$	–	2×10^{10}
CGM Temperature ^a (K)	$1 - 9 \times 10^5$	–	10^6
N Particles	5.5×10^5	8.5×10^4	8.8×10^5

Notes. These values are adopted in the simulations throughout this paper. They differ from L21 in the stellar and gaseous disk masses for the Clouds (lowered to better match observed values), the MW only consists of a DM halo and its corona (for more efficient computation), and the total mass of the SMC has been decreased (to better facilitate the stripping of its ISM into the Trailing Stream).^a The CGM mass and temperature for the LMC is shown as the range of values that we explore in Section 3.

In a subsequent study, the Magellanic Corona was directly observed using absorption line spectroscopy data from the Cosmic Origins Spectrograph on the *Hubble Space Telescope* (Krishnarao et al. 2022). From 28 sightlines extending to 35 kpc away from the LMC, we detected a radially declining profile in high ions (C IV, Si IV, O VI) with a total mass of $1.4 \pm 0.6 \times 10^9 M_{\odot}$ including a warm phase with temperature of 3×10^5 K. These results are consistent with the picture of an LMC embedded within a Magellanic Corona. While these values give us a detailed picture of the LMC’s CGM at the present-day, modeling the evolution of the Magellanic System is needed to constrain the properties of the primordial LMC and its Magellanic Corona.

In this paper, we provide an in-depth exploration of the properties of the Magellanic Corona in the context of the formation of the Magellanic Stream. We present a suite of new simulations with detailed physical models including the self-consistent tracking of star formation, feedback, ionization, and metallicity to directly compare with absorption line spectroscopy observations. We explore the parameter space of temperatures and densities for the Magellanic and Galactic Coronae that provide the best match to the observed properties of the Magellanic Clouds as well as the morphology of the neutral H I Stream. In Section 2, we outline the methodology of our simulations and analysis. In Section 3, we discuss our parameter space exploration of the properties of the Magellanic Corona. Section 4 contains the discussion of our results and the implications for the properties of the MW’s CGM. We conclude in Section 5.

2. METHODS

Our simulation methodology contains three distinct steps. First, we initialize an LMC-mass galaxy (the “ $t = 0$ LMC”; Section 2.2) and run it in isolation (Section 3.1). Once that galaxy has come to equilibrium,

we then set up a new simulation with the MW, SMC, and with that galaxy as our initial LMC (the “pre-infall LMC”). Finally, we let them evolve to their present-day positions and compare with the observed properties of the Magellanic System (Section 3.2). Based on these comparisons with observations, we can determine the best values for our initial LMC and Magellanic Corona (our “fiducial” mass and temperature).

2.1. Simulation Setup

We use GIZMO, a massively parallel, multiphysics code for our simulations (Hopkins 2015; Springel 2005). We utilize its Lagrangian “meshless finite-mass” hydrodynamics scheme which allows for the ability to track individual fluid elements while conserving angular momentum and capturing shocks (Hopkins 2015). Star formation is included (Springel & Hernquist 2003) with a physical density threshold of 100 cm^{-3} , a virial requirement that the gas is locally self-gravitating (Hopkins et al. 2013, 2018), and a requirement that the gas is converging ($\nabla \cdot v < 0$). Mechanical stellar feedback is also included in which we assume a constant supernova rate of $3 \times 10^{-4} \text{ SNe Myr}^{-1} M_{\odot}^{-1}$ for all stars less than 30 Myr old. Each supernova injects $14.8 M_{\odot}$ with 10^{51} ergs of energy and metals following the AGORA model (Kim et al. 2016). Cooling is included down to ~ 10 K following Hopkins et al. (2018) with metal-dependent tables (Wiersma et al. 2009). We don’t include radiative transfer or UV background radiation, however outside the MW at low redshift, we don’t expect these mechanisms to play a significant role.

These simulations improve upon those of L20 and L21 by including accurate star formation and feedback with metallicity and advanced cooling routines. GIZMO calculates self-consistent ionization states for each particle based on collisional heating/ionization, recombination, free-free emission, high and low temperature metal-line

cooling, and compton heating/cooling (see Appendix B in Hopkins et al. 2018) We therefore are able to track the neutral and ionized material separately throughout the simulation.

2.2. Initial Conditions

Table 1 shows the properties of the Magellanic Clouds in our simulation and we used the DICE³ code to generate our initial conditions (Perret et al. 2014). We used an LMC dark matter (DM) mass of $1.75 \times 10^{11} M_{\odot}$ consistent with previous studies (Besla et al. 2012; Pardy et al. 2018; L20; L21) and in agreement with indirect estimations (see Figure 1). We constrained the initial gaseous and stellar disk masses for the Magellanic Clouds by requiring their present-day values to be consistent with observations. This was straightforward for the stellar masses as the stars formed during the simulations comprise only a small fraction of the total. Our $t = 0$ LMC includes a stellar disk of $2.5 \times 10^9 M_{\odot}$. However the gas masses can vary greatly from their initial values due to the tidal interactions and accretion from the Magellanic Corona.

After initializing our Magellanic Corona in DICE with a fixed temperature, we find that it takes ~ 4 Gyr for the system to settle into equilibrium. During this time, 18% of the Coronal gas (in the fiducial case, see below) cools and falls to the center of the potential which increases the gas mass in the galactic disk. This condensation of the Corona forms enough of a gas disk that, at the present day, it is consistent with observations of the LMC. Therefore, we initialize our $t = 0$ LMC with a DM halo, stellar disk, and Magellanic Corona. And after ~ 4 Gyr of evolution in isolation, we find a stable LMC galaxy that we use to represent our “pre-infall” LMC.

In Section 3 below, we explore a variety of masses and temperatures for the Magellanic Corona. In our fiducial case, we initialize our LMC with a Magellanic Corona containing $5 \times 10^9 M_{\odot}$ following an isothermal profile (exponentially truncated at 200 kpc) at a temperature of 3×10^5 K and a metallicity of 0.1 solar. After 3.5 Gyr in isolation, there remains $3.7 \times 10^9 M_{\odot}$ of ionized material bound to the LMC (with $2 \times 10^9 M_{\odot}$ within 120 kpc) with a median temperature of 3.4×10^5 K. $9.1 \times 10^8 M_{\odot}$ has cooled to form the LMC’s gaseous disk. We adopt this as our fiducial “pre-infall” LMC. Radial profiles of density and temperature are shown in Figure 2 in blue.

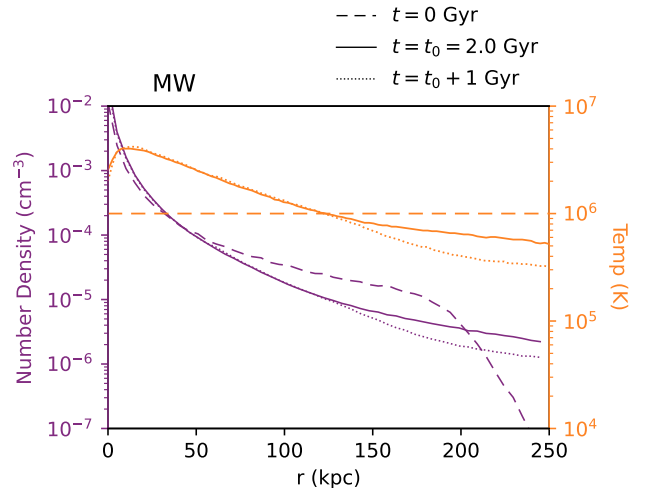


Figure 2. Initial properties of the Galactic Corona. The number density and mean temperature are shown as a function of radius in black and orange, respectively. The dashed lines show the profiles at $t = 0$ Gyr, and the solid lines show the profiles at the end of isolated evolution ($t_0 = 2$ Gyr). The dotted lines show the profiles after an additional 1 Gyr of evolution.

The only constraint on the SMC’s total mass comes from its rotation curve, which requires $2.4 \pm 0.36 \times 10^9 M_{\odot}$ within 4 kpc ($1.25 \pm 0.25 \times 10^9 M_{\odot}$ in DM, Di Teodoro et al. 2019; Stanimirović et al. 2004). However, recent work has shown that the SMC is possibly much more complicated than originally thought (Murray et al. 2023). A variety of SMC masses have been used in previous models ($10^9 - 3 \times 10^{10} M_{\odot}$; Besla et al. 2012; Diaz & Bekki 2012; Pardy et al. 2018; Zivick et al. 2018; De Leo et al. 2020; Patel et al. 2020; Cullinane et al. 2022) and with the inclusion of the Magellanic and Galactic Coronae, we found that lower SMC masses allow for stripped material in agreement with the observations when accounting for realistic heating, cooling, and ionization. In our fiducial model, we used a DM mass of $5 \times 10^9 M_{\odot}$, a stellar mass of $2.5 \times 10^8 M_{\odot}$, and a gaseous disk mass of $1.5 \times 10^9 M_{\odot}$ (listed in Table 1).

For the MW, we implemented a live DM halo with a total mass of $1.1 \times 10^{12} M_{\odot}$ combined with a hot gaseous CGM following a β -profile as in Salem et al. (2015):

$$\rho \propto \left[1 + \left(\frac{r}{r_c} \right)^2 \right]^{-3\beta/2} \quad (1)$$

with $r_c = 0.35$ and $\beta = 0.559$. As with the Magellanic Corona, we explored a variety of models for the Galactic corona as well, which will be discussed in Section 4.1. Our fiducial MW CGM has a total mass of $2 \times 10^{10} M_{\odot}$ at 10^6 K and is nonrotating. After evolution in isolation

³ <https://bitbucket.org/vperret/dice/src/master/>

for 2 Gyr, $1.9 \times 10^{10} M_{\odot}$ remains bound with a mean temperature of 1.4×10^6 K. Figure 2 shows the initial and final (after 2 Gyr in isolation) density and temperature profiles in orange.

We use a mass resolution of $\sim 3 \times 10^4 M_{\odot}$ per particle for the gas elements, $\sim 2 \times 10^4 M_{\odot}$ per particle for the stars, $\sim 10^6 M_{\odot}$ /particle for the DM. This results in a total particle number of 1.5×10^6 . Adaptive softening was used for the gas particles (such that the hydrodynamic smoothing lengths are the same as the gravitational softening length), and softening lengths of 150 pc and 550 pc were used for the stellar and dark matter particles, respectively.

2.3. Orbits of the Clouds

For our simulations including the full interactions between the Clouds and the MW, we used orbital histories very similar to those previously published in L21 including two interactions over ~ 4 Gyr. Our initial positions and velocities were

$$\begin{aligned} r_{i,\text{LMC}} &= (33.03, 584.97, 300.80) \\ v_{i,\text{LMC}} &= (2.24, -63.93, -65.77) \\ r_{i,\text{SMC}} &= (-21.40, 610.74, 357.15) \\ v_{i,\text{SMC}} &= (6.05, 10.48, -109.69) \end{aligned}$$

while the MW was initially at the origin with zero velocity.

3. PROPERTIES OF THE MAGELLANIC CORONA

We explored the parameter space of initial properties of the Magellanic Corona, by varying the initial temperature and total mass. The Corona was initialized with an isothermal distribution. Its total mass (within 200 kpc) ranged from 10^9 to $10^{10} M_{\odot}$. This corresponds to masses of 0.6 and $6 \times 10^9 M_{\odot}$ within the LMC's virial radius of 120 kpc. The initial temperature of the Corona ranged from 10^5 to 9×10^5 K, and we used a metallicity of 0.1 solar. We explored the viability of these different Coronae by determining their stability and their impact on the present-day Stream.

As mentioned above, we initialize our LMC with a DM halo, stellar disk, and the Magellanic Corona. The gaseous disk forms during the first few billion years of evolution (in isolation). The Magellanic Corona is initialized with a streaming fraction of 0.2, meaning it has an azimuthal velocity set to 20% the circular velocity profile. Therefore, when the cooled material collapses onto the disk, it exhibits a bulk rotation as expected. Higher (lower) streaming fractions result in larger (smaller) disks. This is because without any rotation, more material falls into the center of the gravitational potential and high gas densities induce very

strong star formation which blows out the remaining gas. With too much rotation, the infalling cool material spreads out to larger radii (because it has higher angular momentum) and the densities are not high enough for star formation.

3.1. Stability

The main factor in determining the viable parameter space for the temperature and density of the Magellanic Corona is its stability. If the temperature is too high, the Coronal plasma becomes unbound from the LMC and blows off into the Local Group. If the temperature is too low, too much gas falls onto the LMC, leading to disk gas fractions and star-formation rates that are too high compared to observations. Similarly, if the Corona starts with too much mass (i.e. too high density), the LMC disk becomes too gas-rich. Below a certain mass threshold, the Corona remains stable, but in order to reproduce the high ionization fractions along the length of the Stream, the Magellanic Corona must be more massive than $10^9 M_{\odot}$ (within 120 kpc; see Section 3.2).

Figure 3 shows these results. The nine panels depict nine different simulations with varying initial conditions in which the LMC and Magellanic Corona were evolved in isolation. The initial temperature of the Corona increases from left to right (with values of 1, 3, and 9×10^5 K), while the initial mass of the Corona increases from top to bottom (1, 5, and $10 \times 10^9 M_{\odot}$ within 200 kpc). The black lines show the total masses of the gaseous components within 120 kpc (the virial radius of the LMC) as a function of time – total gas mass (solid), ionized mass (circumgalactic Coronal gas; dashed), and neutral disk mass (dotted).

Figure 4 also shows the temperature distribution as a function of radius for the nine simulations at $t = 4$ Gyr. Initial temperature increases to the right and the initial gas mass increases downwards. The mean temperature of the gas within $20 < r < 250$ kpc is shown as a horizontal dashed line. Interestingly, these white lines do not vary dramatically between the three columns. This means that the initial temperature has a minimal effect on the final stable temperature of the Corona.

We do, however, see that increasing the initial mass of the Corona strongly affects the range of temperatures. This is likely related to gas density; the Coronae with higher initial masses contain higher gas densities, which cools more effectively. Cooling is very efficient around 10^5 K, so subtle changes in density and temperature can have a strong impact on the strength of cooling. These higher-density Coronae do not have sufficient supernova energy injection to keep the gas warm, and therefore result in lower temperatures.

Table 2. Pre-infall Properties of the LMC

Model	t_0 (Gyr)	Ionized gas mass		Gaseous disk		Stellar disk	
		Bound ($10^8 M_\odot$)	$r < 120$ kpc ($10^8 M_\odot$)	Mass ($10^8 M_\odot$)	Scale length (kpc)	Mass ($10^8 M_\odot$)	Scale length (kpc)
Fiducial	3.5	37.2	20.2	9.1	2.8	26.7	4.2
Low mass	4.0	9.4	5.2	0.7	1.7	25.1	4.2
High mass	2.5	88.9	36.3	6.1	2.2	30.1	3.7
Low temp	4.0	29.6	21.7	13.6	23.5	29.6	3.8
High temp	4.0	47.0	14.5	0.02	–	26.3	4.0

Notes. Column 1 lists the name of the model (corresponding to the x -axis of Figure 3), Column 2 lists the amount of time the LMC was evolved in isolation, Column 3 lists the amount of bound ionized gas mass (no radius cut), Column 4 lists the ionized gas within the LMC’s virial radius (120 kpc), Columns 5 – 8 list the masses and scale lengths of the gaseous and stellar disks. These are the properties of the LMC before its interactions with the SMC and approach towards the MW.

3.2. Effect on the Magellanic Stream

We now explore the effect of varying the Magellanic Corona’s initial mass and temperature on the properties of the present-day Magellanic System.

3.2.1. Mass

The initial total mass of the Corona directly affects the amount of ionized gas that we observe around the Stream today. Using UV absorption-line spectroscopy and photoionization modeling, Fox et al. (2014) estimated that there is $\sim 1.5 \times 10^9 M_\odot$ of ionized gas associated with the Magellanic System, $\sim 10^9 M_\odot$ of which is in the Trailing Stream region. Figure 5 shows the total mass in the Trailing Stream for various different models. These values were calculated by mimicking the observational technique of integrating the column density at an assumed distance of 55 kpc⁴. These are not the physical masses in the system, but allow us to compare directly with the observational estimates shown in the left-most bar (Brüns et al. 2005; Fox et al. 2014). Continuing from left to right we have the results from the simulations published in Besla et al. (2012) and Pardy et al. (2018) in which no ionized material was produced. The three right-most bars show the results of our simulations for three different initial Corona masses.

The initial LMCs used in these simulations are the “low mass,” “fiducial,” and “high mass” models corresponding to Panels b, e, and h in Figures 3 and 4. The properties of these galaxies after evolving in isolation are listed in Table 2. We take these LMCs and place them at their initial positions with the SMC and MW and allow them to evolve until they reach their present-day

positions. From these simulations, we calculate the total neutral and ionized material in the Trailing Stream; these values correspond to the three right-most columns in Figure 5. Clearly, as we increase the progenitor mass, we reproduce more ionized material in the Stream. For masses below $5 \times 10^9 M_\odot$, we are unable to reproduce the observations. In the models that we tested, either the fiducial or high mass models result in viable ionized gas masses. For higher masses, the LMC’s CGM begins to approach estimates of the MW CGM mass, which is unrealistic given the significant difference in virial masses (a factor of ≈ 10) of the two galaxies. Therefore Magellanic Corona masses below our high mass model value ($\sim 10^{10} M_\odot$) are preferred.

3.2.2. Temperature

We explore the impact of the initial Magellanic Corona temperature on the present-day Magellanic System. As shown in Figure 4, the initial temperature does not have a large effect on the temperature distribution or on the mean Corona temperature after 4 Gyr of evolution. The main difference that we see between temperature models is in the properties of the LMC disk. Because the initial LMC gas disk is formed out of the condensation of the Corona in our isolated equilibrium simulations, the temperature plays a large role in its size and stability.

As above (Section 3.2.1), we have taken our pre-infall initial LMC galaxies and run full simulations of the infall of the Clouds towards the MW. In this case, we are using the “Low temp,” “Fiducial,” and “High temp” models corresponding to Panels d, e, and f in Figures 3 and 4. Their properties are again listed in Table 2.

Figure 6 shows the LMC’s disk at the present day for these three simulations compared with observational data from the HI4PI survey (HI4PI Collaboration et al. 2016; Westmeier 2018). Panels a, b, and c show the results from the low temp, fiducial, and high temp simulations, respectively. Lower initial Corona temperatures

⁴ $M = m_p \Delta x \Delta y \sum N$, where m_p is the proton mass, Δx and Δy are the physical sizes (in cm) of the bin widths in our column density image ($\Delta x = \Delta l_{\text{MS}} \times D$, where D is the assumed distance), and N is the column density.

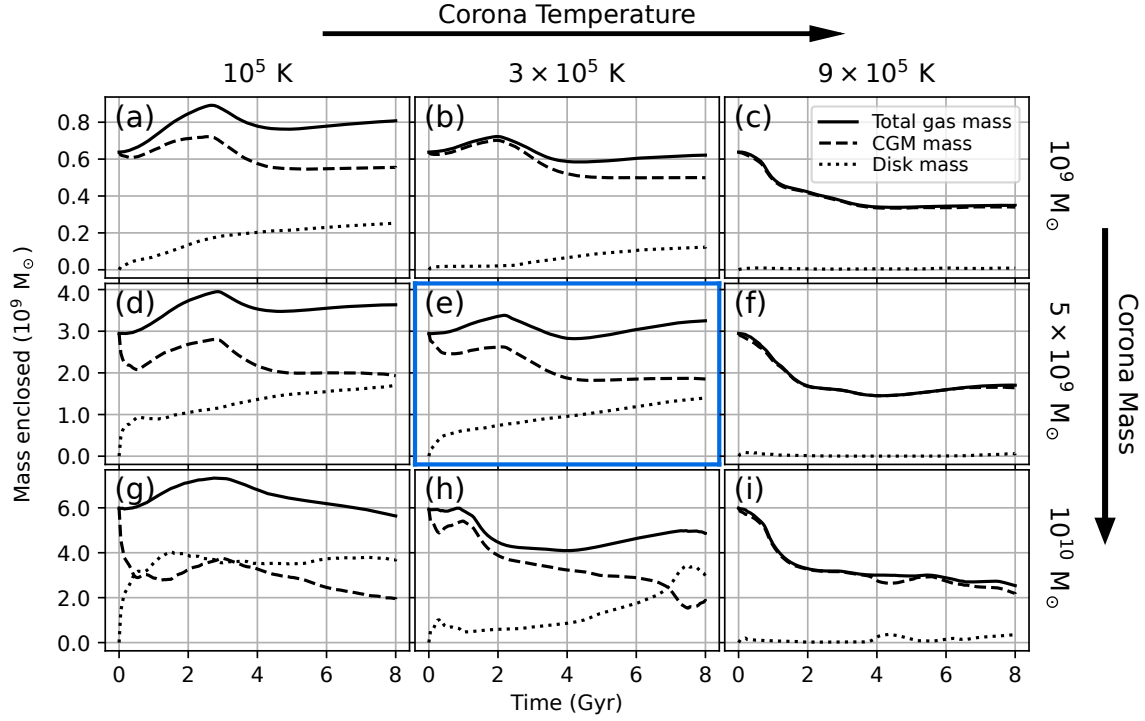


Figure 3. Magellanic Corona stability. Study of the stability of the Magellanic Corona for varying initial masses and temperatures. Each panel shows the total, CGM, and disk masses within 120 kpc as a function of time (solid, dashed, and dotted lines, respectively). The initial temperatures increase from left to right with values of 1, 3, and 9×10^5 K. The initial masses increase from top to bottom with values of 1, 5, and $10 \times 10^9 M_{\odot}$ (within 200 kpc). Our fiducial model (outlined in blue) is the center frame (Panel e) corresponding to an initial mass of $3 \times 10^9 M_{\odot}$ and a temperature of 3×10^5 K. The low and high mass models referenced in Figure 5 correspond to Panels b and h, and the low and high temp models referenced in Figure 6 correspond to Panels d and f.

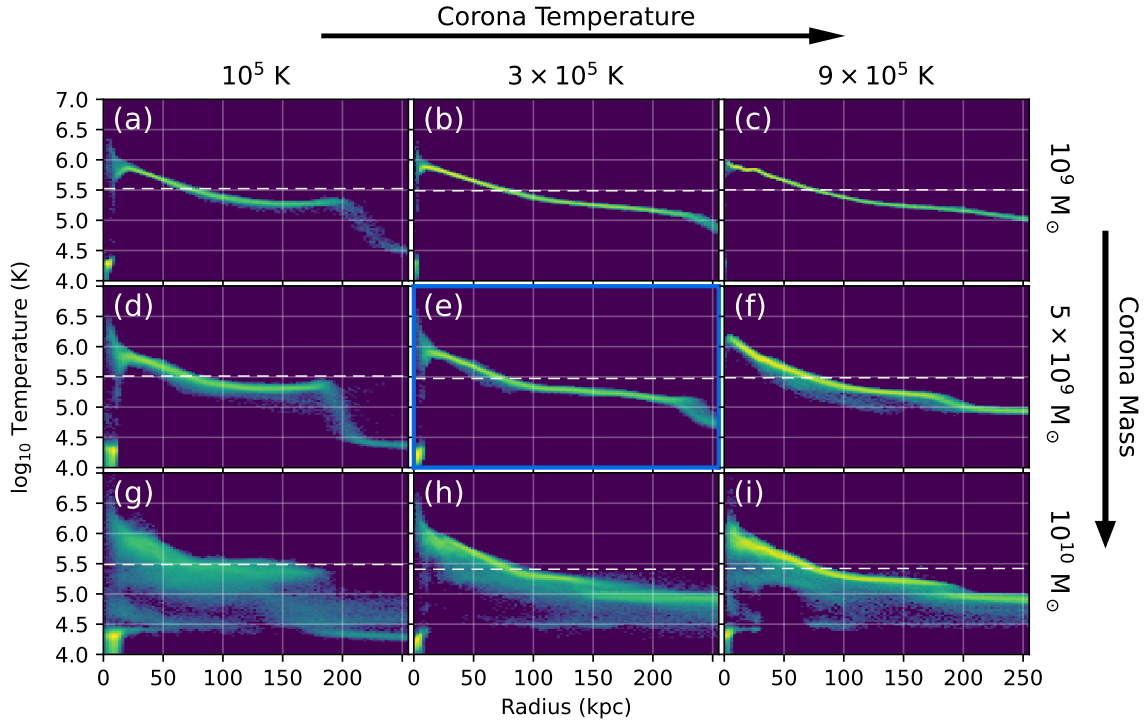


Figure 4. Magellanic Corona temperature. Temperature profile of the Magellanic Corona for nine initial masses and temperatures (as in Figure 3). These histograms show the relative density of the gas temperature as a function of radius for the nine simulations at $t = 4$ Gyr. The horizontal white dashed lines show the mean temperature of the gas within $20 < r < 250$ kpc. Again, our fiducial model is Panel e, outlined in blue.

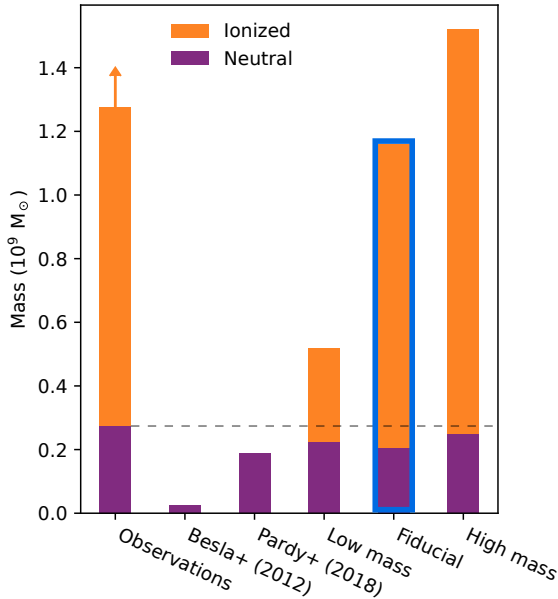


Figure 5. The mass of the Trailing Stream. Each bar shows the results for a different model compared against the observed mass in neutral and ionized gas shown in the left-most column ($2.7 \times 10^8 M_\odot$ in neutral gas, Brüns et al. 2005; $1.0 \times 10^9 M_\odot$ in ionized gas, though this may be an underestimate, Fox et al. 2014). Each value is computed by integrating the column densities for all gas behind the SMC ($l_{\text{MS}} < l_{\text{MS,SMC}}$) assuming a distance to the gas of 55 kpc (as done in observational works, Brüns et al. 2005, Fox et al. 2014). The total neutral masses in Besla et al. (2012), and Pardy et al. (2018) are $2.5 \times 10^7 M_\odot$ and $1.9 \times 10^8 M_\odot$, respectively. The three right-most columns show the results from our new simulations with our low mass, fiducial, and high mass LMCs (each with initial temperature as in the fiducial model; Panels b, e, and h in Figures 3 and 4; see also Table 2). Our fiducial model is outlined in blue (as done in Figures 3 and 4). The neutral material is relatively consistent between these models at 2.2 , 2.1 , and $2.5 \times 10^8 M_\odot$, while the ionized gas masses are 3.0×10^8 , 9.5×10^8 , and $1.3 \times 10^9 M_\odot$ for the three models, respectively. By dividing the ionized mass by the total mass, we can get an approximate value for the average ionization fraction in the Magellanic Trailing Stream, and we find values of 57%, 82%, and 84% for the three models (compared with $\sim 75\%$ in the observed case).

lead to larger LMC disks due to more material cooling and falling towards the center of the gravitational potential. For the highest temperatures (Panel c), no LMC disk forms since the Corona material can’t cool and fall to the center of the gravitational potential. This is also visible in Figure 3f in which the dotted line (showing the total disk mass) remains at zero throughout the simulation and in Table 2 in which the total neutral disk mass is shown to be $2 \times 10^6 M_\odot$.

4. DISCUSSION

The Magellanic Corona model of the evolution of the Magellanic System (L20; L21) has been shown to be a viable candidate for the explanation of the high ionized mass observed (Fox et al. 2014). Strong support for the Corona model is given by the LMC’s high total mass ($> 10^{11} M_\odot$), since a massive LMC can sustain a warm-hot CGM (Jahn et al. 2021). In this work we have explored the physical properties of the Magellanic Corona. We find it has pre-infall masses $\gtrsim 2 \times 10^9 M_\odot$ within the virial radius (Table 2) and gas with temperatures ranging from $10^5 - 10^6$ K (Figure 4).

These results are consistent with previous works quantifying the circumgalactic gas of LMC-mass galaxies in cosmological simulations. Jahn et al. (2021) found circumgalactic gas masses of $3 - 6 \times 10^9 M_\odot$ at temperatures of $10^{4.5} - 10^6$ K for halos with $M_{200} \sim 1.5 \times 10^{11} M_\odot$ in the FIRE simulations (Hopkins et al. 2018), in direct agreement with our findings. Furthermore, Hafen et al. (2019) characterized the CGM of galaxies across a range of halo masses also using the FIRE simulations. For their $10^{11} M_\odot$ halos, they found an average CGM mass of $0.2 f_b M_{200} \sim 3 \times 10^9 M_\odot$.

Recently, Setton et al. (2023) explored the implications of the bow shock generated as the LMC approaches the MW. The envelope of shocked gas could possibly explain some of the ionized gas detections of Fox et al. (2014). Our model presented here does produce some of the same bow shock features including a high temperature leading edge of ionized gas. Because of the inclusion of the Magellanic Corona in our models, there is less of a clear shock boundary, however we are still consistent with the observed H α emission and ionized gas properties.

4.1. Constraining the Milky Way Corona

By exploring the parameter space of temperatures and densities for the MW’s own hot gas corona, we can isolate its effects on the formation and morphology of the Trailing Stream. In this way, we can constrain the CGM properties by comparing our simulations with observations. Inspired by observations (e.g. Anderson & Bregman 2010; Bregman et al. 2018), we varied the total mass from 10^{10} to $8 \times 10^{10} M_\odot$, varied the temperature from 4×10^5 to 3×10^6 K, and tested with and without uniform rotation of the CGM. As we found above with the Magellanic Corona, changing the initial temperature of the gas did not affect the equilibrium temperature distribution significantly. Similarly, rotation, while it did decrease the equilibrium temperature of the CGM slightly, did not have a substantial effect on the Magel-

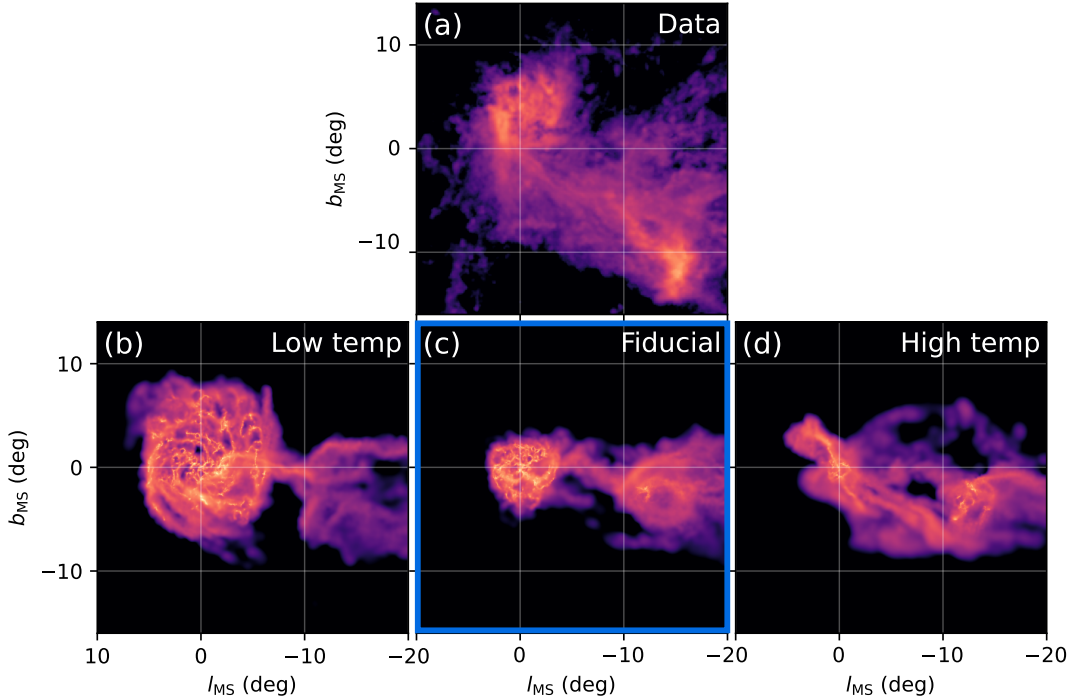


Figure 6. Present-day LMC disk for different Corona temperatures. A zoomed in region around the Magellanic Clouds is shown in Magellanic Coordinates for the observational data (Panel a; HI4PI, Westmeier 2018) compared with three different simulations (bottom panels). Panels b, c, and d show the results from our simulations with low temp, fiducial, and high temp LMCs, respectively (each with its total mass set to the fiducial value; Panels d, e, and f in Figures 3 and 4; see also Table 2). Our fiducial model is outlined in blue (as done in Figures 3 and 4). As the temperature decreases the size of the LMC disk increases due to Corona material collapsing onto the disk. At higher temperatures (Panel d), barely any LMC disk forms.

lanic System. Therefore, the main variable we explored was the total mass.

L21 found that a MW corona mass of $4 \times 10^{10} M_{\odot}$ was required to get the best match to the velocity gradient along the Stream (two times larger than Salem et al. 2015). In the suite of orbits tested in this paper, we found that the largest effect that the MW corona had on the present-day Stream is on the morphology of the neutral and ionized components. Figure 7 shows the ionized (orange) and neutral (grayscale contours) components of the simulated Streams in Magellanic Coordinates for three different models. The total mass of the MW corona increases from top to bottom with values of 1, 2, and $8 \times 10^{10} M_{\odot}$. The higher gas density induces stronger ram pressure on the Magellanic gas, decreasing the on-sky extent of the ionized gas, and making the neutral Stream longer and narrower. We find that a value of $2 \times 10^{10} M_{\odot}$ (Panel b; in agreement with estimates from Salem et al. 2015) provides the best agreement with the observations.

This led to our fiducial MW corona model with a total mass of $2 \times 10^{10} M_{\odot}$ and a temperature of 10^6 K. After 2 Gyr of evolution in isolation, $1.9 \times 10^{10} M_{\odot}$ re-

mains bound to the MW and the coronal gas has a mean temperature of 1.4×10^6 K.

5. CONCLUSIONS

Building on our earlier work (L20; L21), we have characterized the influence of the Magellanic Corona on the formation and evolution of the Magellanic Stream. With this suite of simulations, we have shown that the first-infall Magellanic Corona model of Stream formation can produce a present-day Magellanic System with global properties in agreement with the observations.

We have explored the parameter space of temperatures and densities for the Magellanic Corona to constrain its properties. We find that a pre-infall mass $> 2 \times 10^9 M_{\odot}$ (within 120 kpc) can provide sufficient ionized material at the present day (Figure 5) while being stable around the LMC for long times (Figure 3). In creating our initial conditions for the pre-infall LMC, we found that the initial temperature of the Coronal gas determines the size and mass of the LMC’s gaseous disk. By using a value close to the virial temperature of the LMC’s halo, we find that the Coronal gas remains in equilibrium (with the mean temperature closely matching the virial value; Figure 4) and the LMC’s gaseous

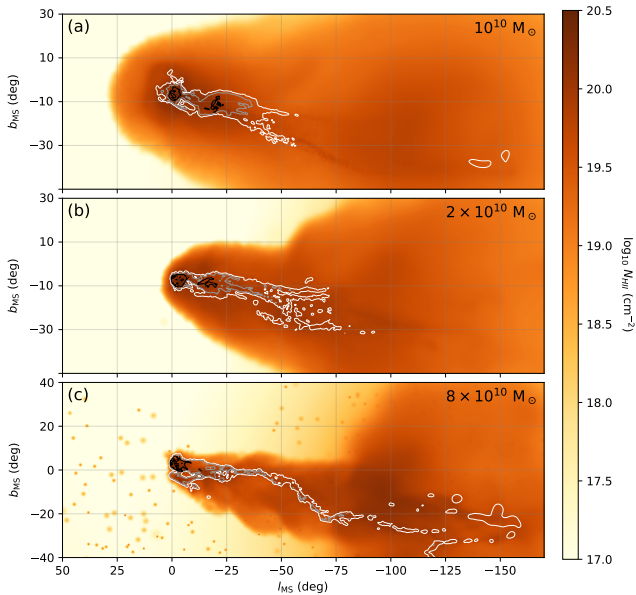


Figure 7. The Effect of the MW Corona on the Present-Day Stream. The ionized (orange) and neutral (grayscale contours) Magellanic gas for three simulations shown as they would appear on the sky in Magellanic Coordinates. Panels a, b, and c, show the results of simulations with a total MW coronal mass of 1, 2, and $8 \times 10^{10} M_{\odot}$, respectively (listed in the top right of each panel). All panels use our fiducial LMC with a Magellanic Corona of $5 \times 10^9 M_{\odot}$ at 3×10^5 K. The neutral gas contours (white, grey, and black) are at values of $\log_{10}(N_{\text{HI}}) = 19, 20,$ and 21 , respectively.

disk at the present day agrees well with the observations. This leads to a pre-infall LMC disk gas mass of $9.1 \times 10^9 M_{\odot}$ with a scale length of 2.8 kpc.

These models can reproduce the properties of observed Magellanic System while accounting for a large LMC mass. The Magellanic Corona provides the key element that necessitates a review of the precise orbital histories of the Clouds. This brings the Trailing Stream gas much closer to us than previously thought, explaining the turbulent morphology and $H\alpha$ brightness, and implying an infall onto the MW disk within ~ 100 Myr.

By obtaining constraints on the distance to the gas in the Stream through absorption-line spectroscopy towards MW halo stars, we will be able to better discriminate between existing models. Moreover, a reevaluation of the properties of the Leading Arm could confirm whether it is Magellanic or not. Further observations like these are needed to constrain key properties of the Magellanic System and to converge on the true history of the Magellanic Clouds.

Support for programs 16363 and 16602 was provided by NASA through a grant from the Space Telescope Science Institute, which is operated by the Association of Universities for Research in Astronomy, Inc., under NASA contract NAS5-26555. The simulations in this paper were run at the University of Wisconsin – Madison Center for High Throughput Computing supercomputing cluster (Center for High Throughput Computing 2006).

Software: astropy (Astropy Collaboration et al. 2013, 2018, 2022), dice (Perret et al. 2014), gala (Price-Whelan 2017; Price-Whelan et al. 2022), pygad (Röttgers 2018; Röttgers et al. 2020), trident (Hummels et al. 2017)

REFERENCES

- Anderson M. E., Bregman J. N., 2010, *ApJ*, 714, 320
- Astropy Collaboration et al., 2013, *A&A*, 558, A33
- Astropy Collaboration et al., 2018, *AJ*, 156, 123
- Astropy Collaboration et al., 2022, *apj*, 935, 167
- Besla G., Kallivayalil N., Hernquist L., Robertson B., Cox T. J., van der Marel R. P., Alcock C., 2007, *ApJ*, 668, 949
- Besla G., Kallivayalil N., Hernquist L., van der Marel R. P., Cox T. J., Kereš D., 2010, *ApJ*, 721, L97
- Besla G., Kallivayalil N., Hernquist L., van der Marel R. P., Cox T. J., Kereš D., 2012, *MNRAS*, 421, 2109
- Bland-Hawthorn J., Gerhard O., 2016, *ARA&A*, 54, 529
- Bregman J. N., Anderson M. E., Miller M. J., Hodges-Kluck E., Dai X., Li J.-T., Li Y., Qu Z., 2018, *ApJ*, 862, 3
- Brüns C., et al., 2005, *A&A*, 432, 45
- Center for High Throughput Computing 2006, Center for High Throughput Computing, doi:10.21231/GNT1-HW21, <https://chtc.cs.wisc.edu/>
- Cohen R. J., 1982, *MNRAS*, 199, 281
- Connors T. W., Kawata D., Gibson B. K., 2006, *MNRAS*, 371, 108
- Cullinane L. R., Mackey A. D., Da Costa G. S., Erkal D., Kuposov S. E., Belokurov V., 2022, *MNRAS*, 510, 445
- D’Onghia E., Fox A. J., 2016, *ARA&A*, 54, 363
- Davies R. D., Wright A. E., 1977, *MNRAS*, 180, 71
- De Leo M., Carrera R., Noël N. E. D., Read J. I., Erkal D., Gallart C., 2020, *MNRAS*, 495, 98
- Di Teodoro E. M., et al., 2019, *MNRAS*, 483, 392
- Diaz J., Bekki K., 2011, *MNRAS*, 413, 2015
- Diaz J. D., Bekki K., 2012, *ApJ*, 750, 36
- Erkal D., Belokurov V. A., 2020, *MNRAS*, 495, 2554
- Erkal D., et al., 2019, *MNRAS*, 487, 2685
- Fox A. J., Wakker B. P., Smoker J. V., Richter P., Savage B. D., Sembach K. R., 2010, *ApJ*, 718, 1046
- Fox A. J., Richter P., Wakker B. P., Lehner N., Howk J. C., Ben Bekhti N., Bland-Hawthorn J., Lucas S., 2013, *ApJ*, 772, 110
- Fox A. J., et al., 2014, *ApJ*, 787, 147
- Fujimoto M., Sofue Y., 1976, *A&A*, 47, 263
- Gardiner L. T., Noguchi M., 1996, *MNRAS*, 278, 191
- Gibson B. K., Giroux M. L., Penton S. V., Putman M. E., Stocke J. T., Shull J. M., 2000, *AJ*, 120, 1830
- HI4PI Collaboration et al., 2016, *A&A*, 594, A116
- Hafen Z., et al., 2019, *MNRAS*, 488, 1248
- Hammer F., Yang Y. B., Flores H., Puech M., Fouquet S., 2015, *ApJ*, 813, 110
- Hopkins P. F., 2015, *MNRAS*, 450, 53
- Hopkins P. F., Narayanan D., Murray N., 2013, *MNRAS*, 432, 2647
- Hopkins P. F., et al., 2018, *MNRAS*, 480, 800
- Hummels C. B., Smith B. D., Silvia D. W., 2017, *ApJ*, 847, 59
- Jahn E. D., Sales L. V., Wetzel A., Samuel J., El-Badry K., Boylan-Kolchin M., Bullock J. S., 2021, arXiv e-prints, p. arXiv:2106.03861
- Kallivayalil N., van der Marel R. P., Alcock C., Axelrod T., Cook K. H., Drake A. J., Geha M., 2006, *ApJ*, 638, 772
- Kallivayalil N., van der Marel R. P., Besla G., Anderson J., Alcock C., 2013, *ApJ*, 764, 161
- Kim J.-h., et al., 2016, *ApJ*, 833, 202
- Kuposov S. E., et al., 2023, *MNRAS*,
- Krishnarao D., et al., 2022, *Nature*, 609, 915
- Lin D. N. C., Lynden-Bell D., 1977, *MNRAS*, 181, 59
- Lin D. N. C., Lynden-Bell D., 1982, *MNRAS*, 198, 707
- Lu L., Savage B. D., Sembach K. R., 1994, *ApJ Letters*, 437, L119
- Lucchini S., D’Onghia E., Fox A. J., Bustard C., Bland-Hawthorn J., Zweibel E., 2020, *Nature*, 585, 203
- Lucchini S., D’Onghia E., Fox A. J., 2021, *ApJ Letters*, 921, L36
- Mathewson D. S., Cleary M. N., Murray J. D., 1974, *ApJ*, 190, 291
- Meurer G. R., Bicknell G. V., Gingold R. A., 1985, *PASA*, 6, 195
- Moore B., Davis M., 1994, *MNRAS*, 270, 209
- Morras R., 1983, *AJ*, 88, 62
- Murray C. E., et al., 2023, arXiv e-prints, p. arXiv:2312.07750
- Nidever D. L., Majewski S. R., Butler Burton W., 2008, *ApJ*, 679, 432
- Nidever D. L., Majewski S. R., Butler Burton W., Nigra L., 2010, *ApJ*, 723, 1618
- Pardy S. A., D’Onghia E., Fox A. J., 2018, *ApJ*, 857, 101
- Patel E., et al., 2020, *ApJ*, 893, 121
- Peñarrubia J., Gómez F. A., Besla G., Erkal D., Ma Y.-Z., 2016, *MNRAS*, 456, L54
- Perret V., Renaud F., Epinat B., Amram P., Bournaud F., Contini T., Teyssier R., Lambert J. C., 2014, *A&A*, 562, A1
- Petersen M. S., Peñarrubia J., 2021, *Nature Astronomy*, 5, 251
- Price-Whelan A. M., 2017, *The Journal of Open Source Software*, 2
- Price-Whelan A., et al., 2022, adrn/gala: v1.6.1, doi:10.5281/zenodo.7299506, <https://doi.org/10.5281/zenodo.7299506>
- Putman M. E., Staveley-Smith L., Freeman K. C., Gibson B. K., Barnes D. G., 2003, *ApJ*, 586, 170
- Read J. I., Erkal D., 2019, *MNRAS*, 487, 5799

- Richter P., Fox A. J., Wakker B. P., Lehner N., Howk J. C., Bland -Hawthorn J., Ben Bekhti N., Fechner C., 2013, *ApJ*, 772, 111
- Röttgers B., 2018, pygad: Analyzing Gadget Simulations with Python, Astrophysics Source Code Library, record ascl:1811.014 (ascl:1811.014)
- Röttgers B., Naab T., Cernetic M., Davé R., Kauffmann G., Borthakur S., Foidl H., 2020, *MNRAS*, 496, 152
- Salem M., Besla G., Bryan G., Putman M., van der Marel R. P., Tonnesen S., 2015, *ApJ*, 815, 77
- Sembach K. R., et al., 2003, *ApJ Supplement*, 146, 165
- Setton D. J., Besla G., Patel E., Hummels C., Zheng Y., Schneider E., 2023, *arXiv e-prints*, p. arXiv:2308.10963
- Sofue Y., 1994, *PASJ*, 46, 431
- Springel V., 2005, *MNRAS*, 364, 1105
- Springel V., Hernquist L., 2003, *MNRAS*, 339, 289
- Stanimirović S., Staveley-Smith L., Jones P. A., 2004, *ApJ*, 604, 176
- Vasiliev E., 2024, *MNRAS*, 527, 437
- Vasiliev E., Belokurov V., Erkal D., 2021, *MNRAS*, 501, 2279
- Wang J., Hammer F., Yang Y., Ripepi V., Cioni M.-R. L., Puech M., Flores H., 2019, *MNRAS*, 486, 5907
- Watkins L. L., van der Marel R. P., Bennet P., 2024, *arXiv e-prints*, p. arXiv:2401.14458
- Westmeier T., 2018, *MNRAS*, 474, 289
- Wiersma R. P. C., Schaye J., Smith B. D., 2009, *MNRAS*, 393, 99
- Zivick P., et al., 2018, *ApJ*, 864, 55
- van der Marel R. P., Kallivayalil N., 2014, *ApJ*, 781, 121